Available online at www.sciencedirect.com
SCIENCE DIRECT®
PERGAMON
International Journal of Heat and Mass Transfer 46 (2003) 4041–4050
International Journal of HEAT and MASS TRANSFER
www.elsevier.com/locate/ijhmt

The growth and collapse of a micro-bubble under pulse heating

Peigang Deng, Yi-Kuen Lee, Ping Cheng *

Mechanical Engineering Department, Hong Kong University of Science and Technology, Clear Water Bay, Kowloon, Hong Kong

Received 17 January 2003; received in revised form 17 April 2003

Abstract

The possibility of using a micro-thermal bubble, generated by a micro-heater under pulse heating, as an actuator for applications in micro-bio-analytical systems is investigated in this paper. The perturbation force, generated when the micro-thermal bubble is formed instantaneously, can be used to promote such actions as mixing in the solution of a micro-reactor. Under pulse heating, a specially designed non-uniform width micro-heater (10×3 μm^2) can induce highly localized near-homogeneous nucleation and results in periodic generation of stable single bubbles in DI water. The single bubble appears precisely on the narrow part of the micro-heater with size restricted within the superheated region in the fluid. The growth and collapse of the bubble, recorded by a high-speed CCD, is shown to be asymmetric with time if the pulse width is at milliseconds in time scale. This asymmetric behavior is very much different from those in thermal ink-jet printers. The bubble behavior under different heating duration, ranging from microseconds to milliseconds, is experimentally studied. A transient 3-D heat conduction numerical simulation is carried out to study the temperature field of the fluid before the nucleation process. To evaluate the perturbation area of the micro-bubble, submicron particles with diameter of 0.96 μm were placed in the fluid and their dynamic response during the transient bubble formation is recorded.

Keywords: Micro-bubble; Micro-heater; Pulse heating

1. Introduction

The growth and collapse of a micro-bubble generated from a micro-heater, with applications to ink-jet printers, has been studied extensively in recent years [1–9]. It has been shown that the pressure inside the bubble could reach several MPa during the initial bubble growth period, and the ink droplet with diameter of micrometer order can be ejected at a velocity of several meter-per-second within a few microseconds [2,3]. Recently, the micro-thermal bubble technology has found new applications in the bio-medical field. Okamoto et al. [10] have successfully ejected DNA segments (presynthesized oligonucleotides) onto a glass surface for DNA micro-array using a bubble jet-printing device. To reduce the high temperature and high shear stress damage to DNA induced by the transient formation of the thermal bubble, they optimized the DNA ejection solvent to improve its volatility, solubility, wettability, viscosity and surface tension by adding special chemicals.

There are many other so-called "lab-on-a-chip" bio-analytical systems under development in recent years. These micro-total-analysis systems (μ-TAS) will all have special features of small size, rapid, inexpensive, and sensitive, which require only a small amount of samples [11]. The drastically reduced size of these micro-bio-analytical devices calls for innovative methods to realize such functions as mixing, separating and churning of fluids, which are easy in a macro-system but difficult in a micro-system because of drastically reduced inertia forces. Much effort has been devoted to develop novel methods to promote these processes in microfluidic devices in recent years [12–14].

In this paper, we investigate the possibility of using a micro-thermal bubble as an actuator for application in bio-analytical systems. It will be shown that the instant formation of micro-bubbles can provide the driving

* Corresponding author. Tel.: +852-2358-7181; fax: +852-2358-1543.
E-mail address: mepcheng@ust.hk (P. Cheng).

0017-9310/03/$ - see front matter
doi:10.1016/S0017-9310(03)00220-5

force for perturbations in the bulk fluid. Under pulse heating, this micro-bubble actuator can generate single micro-bubble periodically at a controllable site with specific size. As an active actuator, it can be used to generate mixing effect in a still reaction chamber without a complicated flow driven system. Also, the micro-bubble actuator has the potential to realize accurate micro-dosing and small amount bio-sample transport. Besides, it can be employed to enhance the kinetics of bio-chemical reactions because perturbations can speed up the collision of molecules in the samples to shorten the reaction time.

It should be noted that most previous studies on micro-bubble behavior under pulse heating were for application to thermal ink-jet printers, where the micro-heater was usually of rectangle shape with size of about 100 μm, and the heating duration at several microseconds. For comparison, our micro-bubble actuator differs from those in ink-jets in two aspects: a below 10 micrometers' size of the micro-heater with a specially designed non-uniform shape, and with typical pulse width of several milliseconds time scale. Due to these differences, the bubble behavior observed in this experiment is different from those of previous ones. Since very few works has been done on bubble generation by pulse heating with pulse width in the range from microseconds to milliseconds, we will study the bubble behavior under such a pulse width range. To evaluate the influencing area of the perturbation force, submicron particles with diameter of 0.96 μm were placed into the fluid, and their dynamic response during the transient bubble formation was recorded. A transient 3-D heat conduction numerical simulation was used to compute transient temperature variation on the heater surface before nucleation occurs and in the fluid to find the optimum design, and to minimize the high temperature damage to the bio-sample.

2. A controllable micro-bubble as an actuator

It is well known that bubbles can be generated either by heterogeneous nucleation or homogeneous nucleation process. Heterogeneous nucleation is a very irregular process. It strongly associates with the pre-existing nuclei on the heater surface, which are in turn depending on roughness, wettability of the heater surface, and the contact angle of the fluid on the heater surface. In other words, heterogeneous nucleation has some random characteristics, which may lead to uncontrollable operation of a micro-bubble actuator. Therefore, to ensure the reliability and controllability of a micro-bubble actuator, it is desirable that the bubble is generated by homogeneous or near-homogeneous nucleation process. In general, when the degree of superheat in the liquid reaches a high enough value, homogeneous nucleation will become the dominant mechanism for the bubble nucleation process. The criterion given by Skripov [15] for the homogeneous nucleation to occur in a boiling process is

$$\frac{\langle \mathrm{d}T/\mathrm{d}t\rangle}{\langle\varphi\rangle^{1/k}[\pi\widetilde{\Omega}_{\mathrm{A}}]^{1/2k}} > T^{*} - T_{\mathrm{s}} \tag{1}$$

where $\langle \mathrm{d}T/\mathrm{d}t\rangle$ is the heating rate, $\langle\varphi\rangle$ a function depending on the superheat and the thermophysical parameters, k the Boltzmann constant, $\widetilde{\Omega}_{\mathrm{A}}$ the number of pre-existing nuclei per unit area on the heater surface, T^{*} the superheat limit of the liquid, and T_{s} the saturation liquid temperature. Skripov's experiment showed that a heating rate as high as $\mathrm{d}T/\mathrm{d}t > 6\times 10^{6}$ K/s was required for homogeneous nucleation around a platinum heating wire, where pre-existing nuclei $\widetilde{\Omega}_{\mathrm{A}}$ was assumed to be $10^{6}/\mathrm{cm}^{2}$. Since a rapid temperature rising rate of the heater is necessary for homogeneous bubble nucleation, the feature size of the heater should be as small as possible. Therefore, the feature size of the micro-heater in this study was chosen to be at several micrometers. Moreover, the micron size scale of the heater can provide a highly localized heating in order to place as little heat as possible so that the high temperature zone would not be too large that would damage the bio-sample.

The appearance of a vapor bubble in the fluid can induce two kinds of fluid motion at opposite directions: a source flow is generated when a bubble grows where fluid flows outwardly from its center, and a sink flow is generated when the bubble collapses where fluid flows towards its center. Assuming that the fluid is incompressible, the continuity equation (1-D spherical coordinates) shows that the velocity of the fluid is

$$V_{\mathrm{l}} = \frac{\mathrm{d}r}{\mathrm{d}t} = \frac{\mathrm{d}R}{\mathrm{d}t}\frac{R^{2}}{r^{2}} = \dot{R}\frac{R^{2}}{r^{2}} \tag{2}$$

where V_{l} is the fluid velocity at a radius equal to r, t time, R bubble radius, $\dot{R}$ bubble interface velocity at $r = R$. Obviously, if the bubble growth velocity is equal to the bubble collapse velocity, there will be no net fluid flow after one cycle of bubble growth and collapse period, assuming that the wall effect is neglected and no bubble departs. In other words, the perturbation effect in the fluid in such a case will be ineffective. It should be noted that most previous researches on bubble generation under pulse heating show a nearly symmetric bubble growth and collapse periods [3,4], where the width of the heating pulse was kept at several microseconds. In general, the bubble growth period is comparable to the pulse heating duration while the bubble collapse period is determined by the condensation process in the later stage of bubble lifetime. For transient heating, a relatively long heating duration would result in a relatively large heated area in the fluid and more thermal energy would be stored in the fluid. This in turn would result in

a longer vapor bubble condensation process and also the bubble collapse period. Therefore, a relatively long pulse heating duration can change the near-symmetric bubble growth–collapse pattern (under microsecond-wide heating pulse) by prolonging the vapor bubble condensation process. Thus, a typical heating pulse width at millisecond level was chosen in this experiment.

3. Design and fabrication of micro-heater

Fig. 1a is the picture of a specially designed non-uniform micro-heater with a slim part in the middle section that was manufactured by MEMS technology. This micro-heater differs from a conventional strip heater with uniform width as shown in Fig. 1b. In both designs, Pt was chosen as the material for the heater and Au for the electric pad. It is well known that isotherms in a heat conduction problem with inner heat source are of parabolic shape. The heater with non-uniform width can concentrate the electric power at the narrow part of the heater, and therefore drastically increases the heat generated per unit volume there. This highly localized heating would result in a much sharper parabolic temperature distribution as will be discussed in the numerical simulation later. The specially designed heater consisted of two parts as labeled in Fig. 1a: the two side parts (A) was used to warm up the surrounding liquid, while the slim part (B) provided the energy to generate the thermal bubble. Normally, cavities may exist at the overlapped joint of the Pt and Au thin films because of the imperfect fabrication process. A subtle reason for choosing such a design is that the one-step fabrication process of the heater can ensure a smooth contact of the high temperature area of the heater (part B) with the mid temperature area (part A), and the cavities at the joint of the heater and the electric pad can be restricted to the outside of the high temperature area on the heater surface. This is an important consideration for the design of a micro-bubble actuator when controllability of bubble dynamics is required.

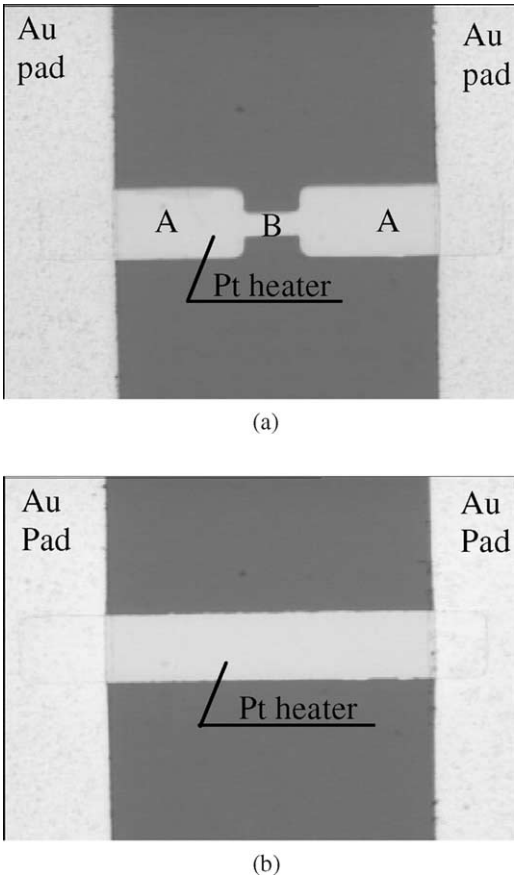

Fig. 1. Picture of two micro-heaters: (a) specially designed non-uniform micro-heater; (b) conventional strip micro-heater.

For comparison purposes, two different designs of the micro-heater, the non-uniform one and the conventional strip one, were fabricated and experimentally tested. The length and width of the strip heater were 50 and 10 μm respectively. For the non-uniform heater, the length and width of part A were 20 and 10 μm, and those of part B were 10 and 3 μm respectively. The fabrication process of the micro-heaters followed the conventional MEMS technology. A p-type, double-sided polished, and ⟨1 0 0⟩ oriented Si wafer (4 in. in diameter and 400 μm in thickness) was used as the substrate. The wafer was coated with 0.5 μm silicon oxide and 1 μm low stress silicon nitride on both sides of the wafer by dry thermal oxidation and low-pressure chemical vapor deposition (LPCVD) process respectively. A 0.02 μm thick Ti film and 0.1 μm thick Pt film were sputtered on the wafer and patterned using the lift-off method. This technique was adopted because the directional randomness of the sputtering process resulted in good granular structure that further led to an accurate thickness (concentration) control. Finally, a 0.2 μm thick Au film was sputtered after a 0.01 μm thick TiW sputtering, and patterned also by the lift-off method. The length and width of the Au pad were both 300 μm.

4. Transient 3-D heat conduction model

We now perform a numerical simulation on temperature distribution near the heater just before the nucleation process. The governing equation of transient 3-D heat conduction with inner heat source is

$$\rho c_{\mathrm{p}} \frac{\partial T}{\partial t} = k\left(\frac{\partial^2 T}{\partial x^2} + \frac{\partial^2 T}{\partial y^2} + \frac{\partial^2 T}{\partial z^2}\right) + \dot{\Phi} \tag{3}$$

where T, ρ, c_{p}, k, t and $\dot{\Phi}$ are temperature, density, isobaric heat capacity, thermal conductivity, time and

the inner heat source per unit volume respectively. It should be noted that the heat dissipation of the gold electric pad, $\dot{\Phi}$, was ignored because it is much smaller compared with that of the platinum heater. With the effect of temperature in the platinum resistance taken into consideration, $\dot{\Phi}$ of the heater is expressed as

$$\dot{\Phi} = I^2 R / V_R = I^2 R_0 [1 + \alpha(T - T_0)] / V_R \quad (4)$$

where I, R and V_R are the current, resistance and the volume of the heater, α the temperature coefficient of the Pt resistor, and R_0 the resistance at a reference temperature T_0. For this computation, α was chosen to be 0.0039 1/K, and R_0 was determined from $R_0 = R_{sheet}(L/W)$ where R_{sheet} is the sheet resistance of the Pt; L and W are the length and width of the heater respectively. The sheet resistance was measured after Ti and Pt sputtering and for our case it was 0.6 Ω/square. DI water was chosen as the working fluid. Some material properties used in the model are listed in Table 1.

Fig. 2 is a schematic diagram of the numerical model. Since the heater is horizontally symmetric, only half of the heater was employed as the computation domain in x–y plane, as indicated by the dot line square (0–A–B–C) in Fig. 2a. Due to the transient heating process and the much smaller heater size, heat conduction could only take effect within a small area around the heater. Therefore, the boundary conditions in x–y plane were: the temperatures at B–C, C–0 and 0–A planes were at room temperature 25 °C, while at A–B plane the adiabatic condition $\partial T/\partial x = 0$ was applied. In z direction, temperatures at the bottom surface of the silicon and at the top surface of the water were at room temperature 25 °C. The temperatures in the whole computation domain were at room temperature initially. Since the sputtering technique was adopted for metal fabrication, a good thermal contact between the heater and the electric pad was assumed. Thus, the interface thermal contact resistance was ignored.

4.1. Results and discussions

Eq. (3) was numerically solved by a finite difference method with the implicit scheme. To comply with experimental conditions, the input current in Eq. (4) was chosen to be the onset current for bubble generation in the experiment, which was 0.08 A for the non-uniform heater and 0.245 A for the strip heater. The corresponding input power was 28.2 and 180.1 mW for the non-uniform heater and the strip heater respectively.

Table 1
Material properties

	Thermal conductivity (k) W/m °C	Heat capacity (c_p) J/kg °C	Density (ρ) kg/m^3
Silicon oxide	1.4	840	2070
Silicon nitride	1.67	714	3200
Platinum	73	133.1	21500
Gold	315	128.7	19280
DI water	0.609	4180	1000

4.1.1. Temperature distribution at the end of the pulse

A 1.6 ms wide heating pulse was adopted for simulation, which was a typical pulse hearing width used in the experiment. Fig. 3 shows the 2-D temperature distribution on the heater surface. From the figure, we can see that the maximum temperature for bubble generation was 214 °C on the non-uniform heater and 204 °C on the strip heater. Along the transversal centerline of the heater surface (insert A–A view in Fig. 3), the temperature distribution for a conventional strip heater was still of parabolic shape, while the non-uniform heater was able to change the shape of this profile and made it much sharper in the slim part as predicted before. The high temperature area (over 100 °C) on the non-uniform heater was 12×3 μm^2, while on the strip heater was 52×10 μm^2. As expected, the non-uniform heater can limit the high temperature to a very small area on the heater surface, which is a little bigger than the slim part (part B in Fig. 1a) of the heater. This is the reason why the input power for the non-uniform heater was much smaller than that of the strip heater.

4.1.2. Transient temperature response

Fig. 4 shows the transient maximum temperature at different depths in the fluid when the heater was turned on. It can be estimated from the figure that the average

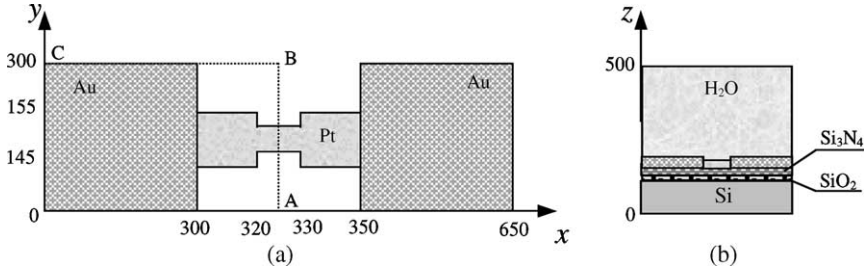

Fig. 2. Schematic diagram of the computation model: (a) x–y plane, unit: μm; (b) z direction, unit: μm.

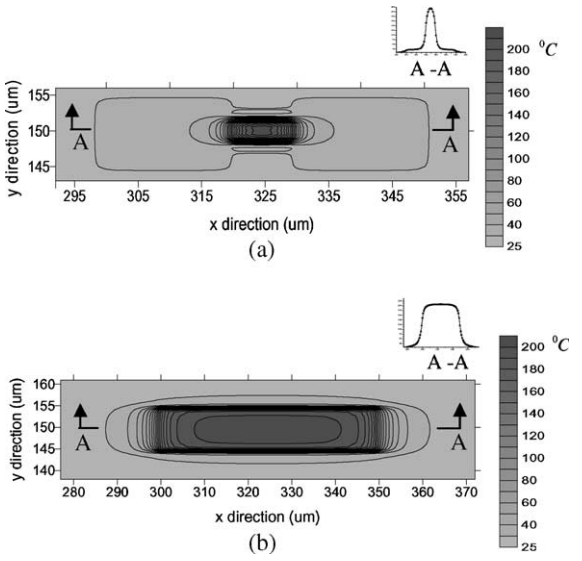

Fig. 3. Two-dimensional temperature distribution on the heater surface at the end of a 1.6 ms pulse heating: (a) non-uniform heater, $I = 0.08$ A; (b) strip heater, $I = 0.245$ A.

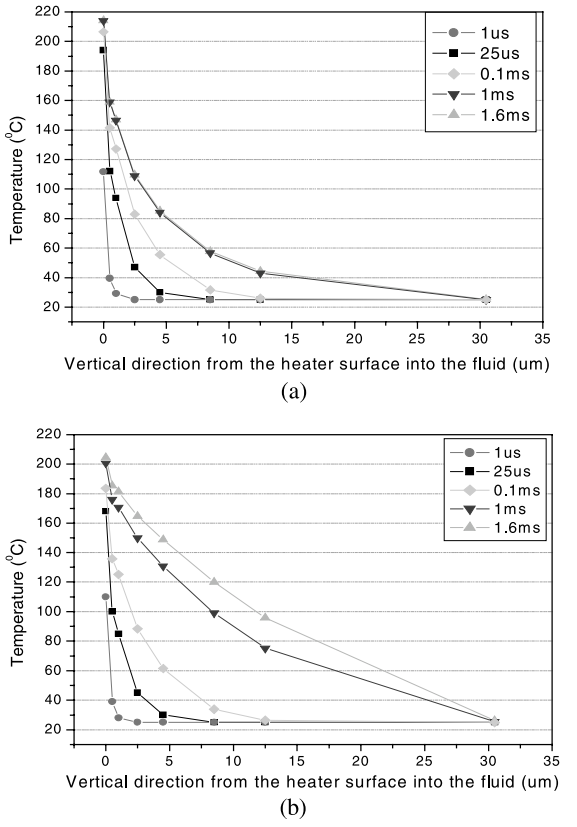

Fig. 4. Transient maximum temperature at different depths in the fluid: (a) non-uniform heater, $I = 0.08$ A; (b) strip heater, $I = 0.245$ A.

temperature rising rate of the non-uniform heater was of the order of 10^6 K/s for nucleation, which was in the same order of magnitude as the homogeneous nucleation on a platinum heating wire as discussed in Section 2. Moreover, both heaters can reach a maximum temperature of above 100 °C within less than 1 μs. However, to reach 200 °C, the non-uniform heater needed about 0.1 ms, while the strip heater needed about 1 ms. Thus, the non-uniform heater had a faster thermal response than that of a conventional strip heater.

Within the first several microseconds after heating, the maximum temperature profiles at different depths seemed very similar for both heaters. However, a large difference in temperature began to appear after a sufficiently long time. The temperature decayed exponentially into the fluid for a non-uniform heater, while it decayed almost linearly for the strip heater. Thus, the non-uniform micro-heater was able to limit the high temperature influence in a small region, both in x–y plane and z direction, which is of great importance for bio-applications. Fig. 4a also shows that the heated area in the fluid is much larger at 1.6 ms than that at 1 or 25 μs, and this enlarged heated liquid layer will prolong the vapor bubble condensation process when the bubble collapses as will be discussed in Section 5.2.2.

5. Experiment

Fig. 5a is a photo of the micro-thermal bubble actuator, and Fig. 5b is a SEM picture of the micro-heater. The chip was mounted on a PCB, and the electric pad on the chip was wire bonded to the PCB. DI water was put onto the chip surface by a pipette, and contacted the micro-heater directly. Fig. 6a is the schematic diagram of the experimental set-up, where a high speed CCD camera (PCI 8000s, MotionScope) was connected to a microscope, and was synchronized with the heating process. Limited by the sensitivity of the CCD, its maximum speed was 2000 frames per second. The heating pulse was provided by a switching circuit, which could provide pulse width as short as several microseconds.

5.1. Control circuits

The control circuit for the pulse heating is schematically shown in Fig. 6b. A programmable 8255 I/O card was employed to generate a pulse train, which was sent to the base of a high gain transistor (ZTX689B, Zetex) to control the on/off of the heating process and was also sent to the CCD camera to trigger the recording process. According to the data sheet, the switching time of the transistor was at nanosecond level. A DC power supply (DC power supply DF1731SB, Goldsource) and the micro-heater were connected to the collector of the

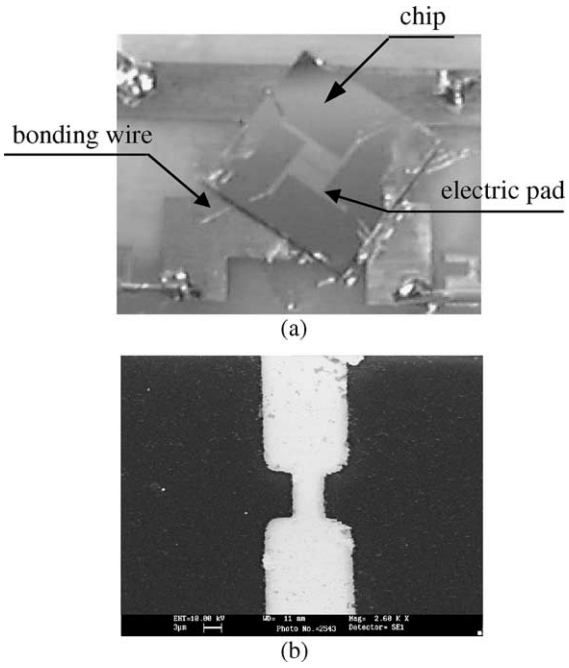

Fig. 5. Picture of the micro-thermal bubble actuator: (a) packaged micro-thermal bubble actuator; (b) SEM picture of the non-uniform micro-heater.

transistor, and the emitter was grounded. The pulse width, τ_1 in Fig. 6b, varied from several microseconds to milliseconds, and to avoid the overlapping of bubbles, a waiting pause, τ_2, was inserted between two consecutive heating pulses. Since the CCD camera recording was synchronized with the heating process, the recording process and the heating process were simultaneous.

5.2. Results and discussions

5.2.1. Visualization of micro-bubble nucleation

When the energy input from a 1.6-ms-width heating pulse to the non-uniform heater reached a critical value of 28.2 mW (0.08 A) for the onset of bubble generation, single bubbles could be observed clearly, stably and repeatedly on the heater surface. Fig. 7 shows a series of snapshots taken by the high-speed CCD camera at different times during the micro-bubble generation, growth and collapse process in DI water. From the video, we can see that micro-single bubble generated precisely on the slim part of the non-uniform heater, and then it grows rapidly until reaching its maximum size. This process lasted about 2 ms in this experiment. It should be noted that due to the limitation of the CCD recording speed, 2 frames per millisecond, some information was lost during this rapid growing process. After reaching its maximum size, the single bubble collapsed, which was a much longer process (about 310 ms in this experiment), comparing to the bubble growing process. This unique phenomenon will be discussed in detail in next section. No bubble departure was observed in the repeating tests in this experiment because of the short heating time.

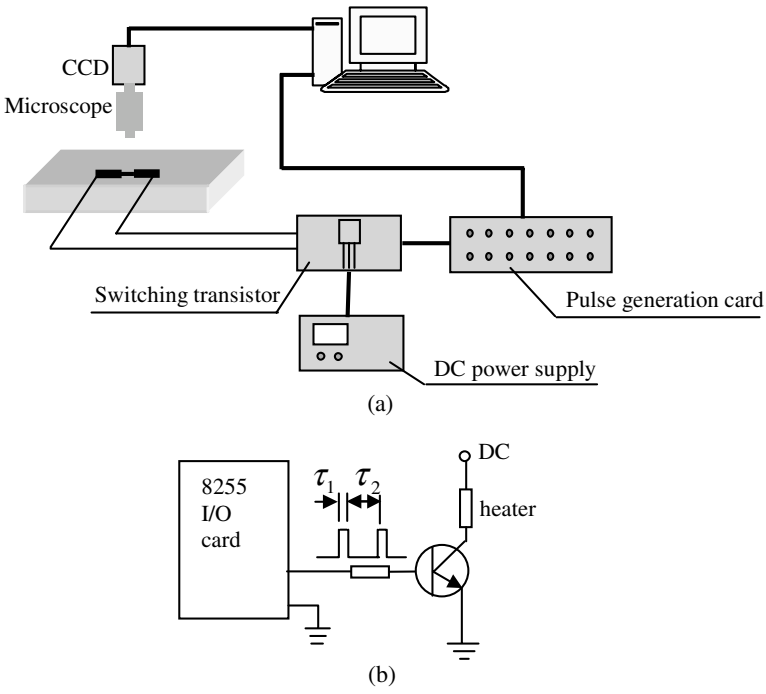

Fig. 6. (a) Schematic diagram of the experimental set-up and (b) the control circuit of the micro-heater.

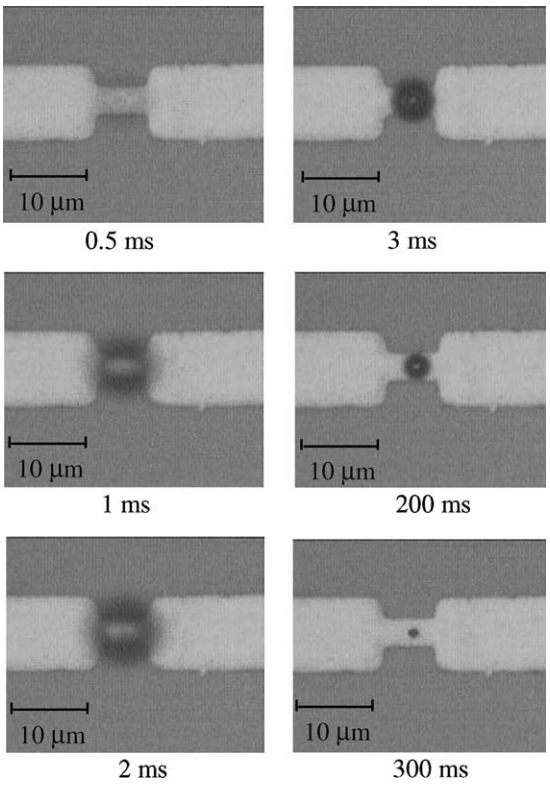

Fig. 7. Micro-single bubble observed in DI water on the non-uniform heater. The pulse heating power was 28.2 mW, and the pulse width was 1.6 ms.

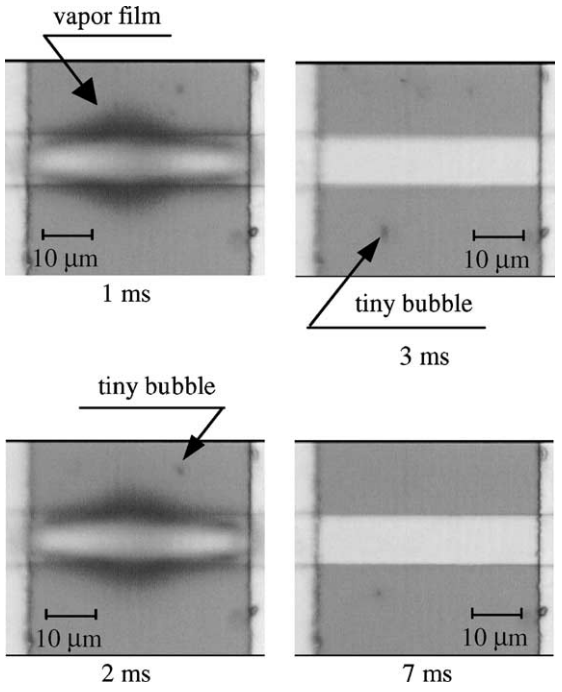

Fig. 8. Boiling on the strip heater. The pulse heating power was 180.1 mW, and the pulse width was 1.6 ms.

Fig. 8 shows the pictures taken during the boiling process on the micro-strip heater under pulse heating with pulse width also being kept at 1.6 ms, where the energy input was 180.1 mW (0.245 A) for the onset of boiling. It was observed that a thin film boiling process was formed on the strip heater where the superheated area was much larger than that on the non-uniform heater (Fig. 3). Comparing with the pictures in Fig. 7, no stable bubbles can be observed during the film boiling process, except that some tiny bubbles appeared instantaneously at random sites.

The fact that a single bubble can be generated at a controllable location can be attributed to the specially designed non-uniform micro-heater, because it can provide a fast and highly localized heating at a specific location in the fluid. According to molecular kinetics, the energies of liquid molecules are not equal and are considered to follow a certain regular distribution [16]. Thus, the density of the liquid at different spaces will fluctuate around an average value due to the non-uniform energy distribution of the liquid molecules. The random accumulation of those molecules, having relatively larger energy than the other molecules, will induce a temporary and local low-density area in the bulk liquid. This "empty place" is regarded as nucleation nucleus, embryo of the micro-bubble. In our experiment, the pulse heating led to a localized superheated area of $12\times3\times4$ μm^3 in the liquid, which increased the mean level of the energy fluctuation of the liquid molecules there. When nucleation occurred (the first frame in Fig. 7), the micro-heater was heated up to about 200 °C (Fig. 4a) at a heating rate of the order of 10^6 K/s. This highly localized and fast thermal energy input resulted in a fast kinetic energy increase of the liquid molecules in the small superheated zone, which quickly resulted in a local near-homogeneous bubble nucleation process. From the SEM picture of the micro-heater (Fig. 5b), it shows that there were no noticeable cavities on the heater surface except for some peeling of the Pt thin film at the edges. Therefore, the fact that the degree of superheat required for the bubble nucleation (about 100 °C) was much larger than that for a heterogeneous boiling, and there were no noticeable pre-existing cavities on the heater surface also suggest that the single bubble generation on this non-uniform width heater was a local near-homogeneous nucleation process.

5.2.2. Single bubble dynamics

In order to characterize single bubble dynamics quantitatively, the bubble diameter in each frame of the digitalized video was measured using a Matlab program. Based on the recorded pictures as partly shown in Fig. 7,

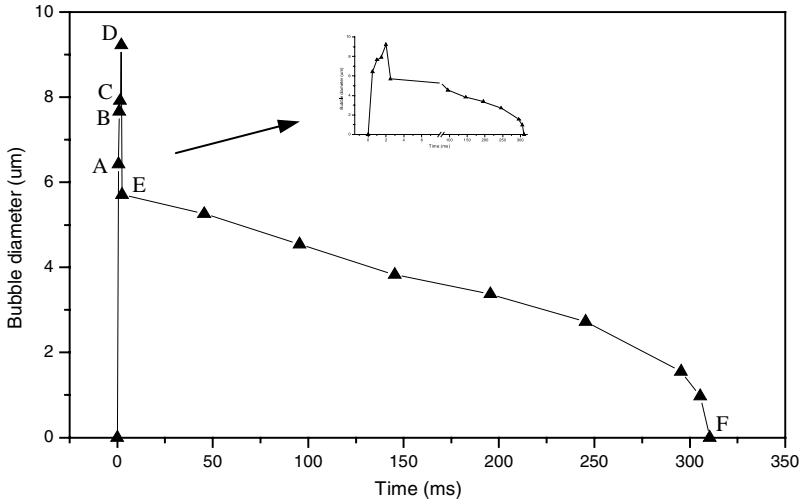

Fig. 9. Single bubble diameter versus time. The pulse heating power to the non-uniform heater was 28.2 mW, and the pulse width was 1.6 ms.

the bubble diameter as a function of time covering the entire bubble generation and collapse process could be obtained. The results are presented in Fig. 9. Due to the limitation of the recording speed of the CCD camera, only four frames were taken during the rapid bubble growth period, which are labeled as A, B, C, and D (max size) in the figure. The pressure inside the initial microbubble was supposed to be the saturation vapor pressure at the temperature of bubble generation, which was about 200 °C according to Fig. 4a. Therefore, the initial pressure difference at the vapor and liquid interface of the bubble was approximately 1.45 MPa, most of which should be balanced by the surface tension according to the near-thermodynamic equilibrium condition at the vapor liquid interface:

$$p_v - p_l \approx 2\sigma/R \tag{5}$$

where p_v and p_l are vapor pressure and liquid pressure, σ surface tension, and R initial bubble radius. The bubble growth would accelerate with increase in bubble size as the surface tension is reduced. At the same time, the pressure inside the bubble would slowly dissipate due to the work of expansion as the bubble grew. Note that bubble growth at this initial stage was mainly controlled by dynamic forces [17]. At the later stage, when the pressure difference and the inertia of the surrounding liquid became small, bubble growth was governed by the rate at which heat could be supplied from the superheated liquid layer to the bubble interface to facilitate the vaporization process [18,19]. It is pertinent to note that the whole bubble growth period was highly affected by the non-uniform temperature distribution of the liquid surrounding the vapor bubble, as will be discussed later. Points A (0.5 ms), B (1 ms), C (1.5 ms) and D (2 ms) labeled in Fig. 9 were the snapshots corresponding to the whole bubble growth process. Note that the heating pulse was stopped at 1.6 ms (shortly after point C). The continuing growth of the bubble after heating, C to D in Fig. 9, was because of the inertia effect. The maximum diameter of the bubble measured in this experiment was 9.2 μm, which was very close to the size of the superheated zone in the fluid ($12\times3\times4$ μm^3).

After the bubble reaching its maximum size at D as shown in Fig. 9, it started to collapse on the heater surface. A sudden drop of the bubble size, from D to E, was always observed in the repeating runs, which made the whole collapse process discontinuous. The continuing expansion of the bubble volume at the end of the heating pulse actually was at the expense of the vapor pressure inside the bubble, i.e., internal energy was consumed to compensate for the expansion work. Thus, a negative pressure difference was established between the vapor and liquid interface of the bubble, which would reach the maximum value when the bubble size was maximum. Moreover, this was also the moment at which the acceleration of bubble collapse reached the maximum value, which explained the sudden drop of the bubble size as it started to shrink. In fact, this rapid bubble collapse was very similar to the rapid growth as the bubble was initially generated. Both of these processes were dominated by dynamic force (pressure), but with the direction of the acceleration reversed. After the sudden collapse of the bubble, the pressure difference would be small, and the subsequent bubble collapse was then mainly dominated by the vapor condensation in the subcooled liquid.

A unique characteristic of the bubble dynamics observed in the present experiment is its distinct asymmetry

lifetime of the bubble growth and collapse process (Fig. 9): about 2 ms for the former and 310 ms for the latter. As mentioned in Section 2, previous studies [3,4] of bubble dynamics under pulse heating showed a near-symmetric bubble growth and collapse process, where the heating pulse width was kept at microsecond level. For example, Asai [3, Fig. 7] performed an experiment using heating pulse widths varying from 5.2 to 52 μs, which showed near-symmetric bubble growth and collapse periods. The different behaviors of the symmetry and asymmetry bubble dynamic may be explained by the different duration of the heating pulse widths. In our experiment the heating pulse width was 1.6 ms, which was much longer than that used in Asai's experiment. A relatively long heating duration of the heater surface to the fluid enabled more thermal energy being accumulated in the fluid, resulting in a larger heated zone in the fluid (as shown in Fig. 4a). This will in turn prolong the condensation process of the vapor bubble when it collapses.

Fig. 10 shows the bubble diameter with respect to time under heating pulse widths from 0.015 to 5 ms. When the pulse heating duration was in the range of 0.015–0.18 ms, single bubble could still be observed on the heater surface, but only a few pictures were captured due to the limitation of the CCD's speed. When the heating pulse duration was in the range of 0.85–5 ms, the bubble growth and collapse patterns were very similar to each other. An asymmetric bubble dynamic was still observed as well as the sudden drop of the bubble size at the beginning of the collapse. It is clear to see that the longer the heating pulse duration the longer the bubble collapse period, which is consistent with our discussion above. This figure can be used to analyze the operation frequency of the bubble actuator, because the bubble lifetime will determine its working period. For example, under a 1.6 ms wide heating pulse, the maximum working frequency of the bubble actuator will be about 3 Hz.

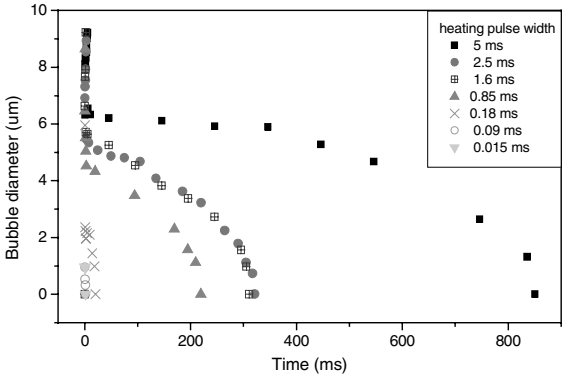

Fig. 10. Effect of heating pulse width on bubble diameter variation with time.

5.2.3. Perturbation force

To evaluate the influencing area of the perturbation force, submicron particles of 0.96 μm in diameter were placed in the DI water to trace the movement of the fluid, and their dynamic response was recorded by a high speed CCD camera. From the digital video recorded, the movement of the tracing particles during the bubble lifetime is clearly shown. Some snapshots selected from the video are presented in Fig. 11. Before bubble generation, the particles suspended in the fluid and vibrated randomly. At the early stage of bubble growth period, the particles moved drastically away from the bubble, which corresponded to the source flow pattern as discussed in Section 2. Due to the initial large pressure difference between the inside and outside of the bubble interface (the difference of the saturation vapor pressure at 200 °C and the ambient pressure was 1.45 MPa), the particles moved at high accelerations until the bubble reached a maximum size. The subsequent sudden shrink of the bubble volume led to a sink flow, and the particles moved back as a consequence. Because of the asymmetry of the bubble expansion and collapse process (Fig. 9), a net displacement of the particles was achieved. It should be noted that the particles returned to their free vibration stage during the long collapse process after a sudden shrink. The effective perturbation region was assumed to be a semi-sphere with its center at the center of the bubble, and it could be evaluated by estimating the net displacement of the particles. From the visualization

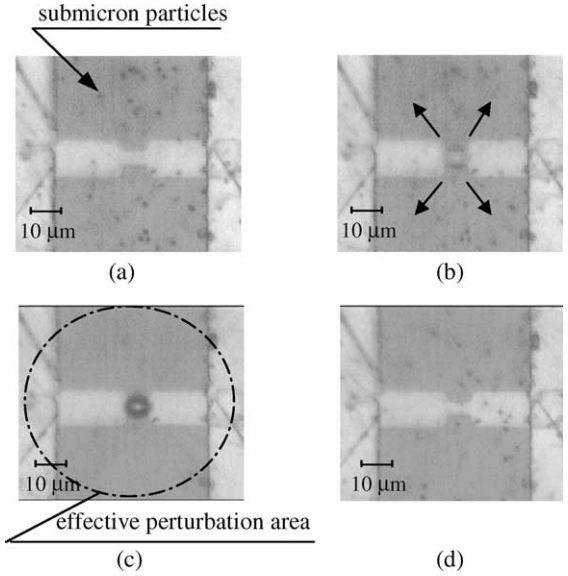

Fig. 11. Dynamic response of the submicron particles: (a) before bubble generation; (b) particles begin to move at the initial stage of bubble formation; (c) bubble growth stage; (d) after bubble collapse.

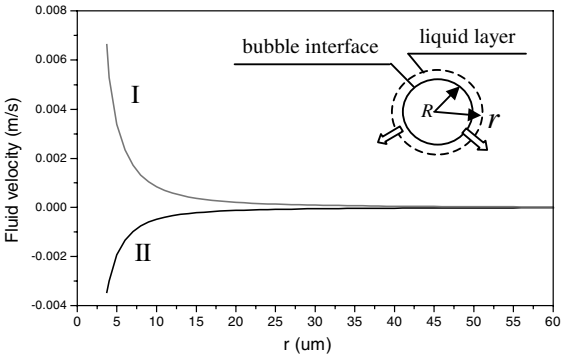

Fig. 12. Fluid velocity at different radius as bubble grows and collapses. Curve I: at the initial stage of bubble growth, where $\dot{R} = 0.0066$ m/s; Curve II: at the initial stage of bubble collapse, where $\dot{R} = 0.0035$ m/s.

study, the radius of the perturbation was estimated as six folds of the maximum bubble radius.

Based on Eq. (2) and the experimental data of bubble size as a function of time, we can obtain the bulk fluid velocity during bubble growth and collapse periods, as presented in Fig. 12. The fluid near the bubble interface had a maximum velocity of 0.0066 m/s when bubble began to grow and 0.0035 m/s when bubble began to collapse.

6. Concluding remarks

A specially designed non-uniform width micro-heater, for application in bio-analytical field, was fabricated using MEMS technology. This micro-heater has a fast thermal response time and can restrict the high temperature zone of the fluid to a very small region adjacent to the heater. Owing to the highly localized and fast pulse heating from the heater surface to the fluid, near-homogeneous bubble nucleation was initiated, which finally resulted in a stable periodic generation of single bubbles. The size of the micro-single bubble was comparable to the feature size of the heater, as well as the superheated zone in the fluid. The bubble growth period was comparable to the width of the heating pulse, and the bubble collapse was essentially a long thermal control process. Because of the asymmetry of the bubble expansion and collapse periods, effective perturbation can be achieved in the bulk fluid. Visualization shows that the radius of the perturbation was about six folds of the maximum bubble radius. Thus, periodic generation of single micro-vapor bubbles appears promising to be used as an actuator for applications in micro-bio-analytical systems.

Acknowledgements

This work was supported by the Hong Kong Research Grant Council through RGC grant HKUST6014/OE2.

References

[1] R.R. Allen, J.D. Meyer, W.R. Knight, Thermodynamics and hydrodynamics of thermal ink jets, Hewlett-Packard J. 36 (1985) 21–27.
[2] A. Asai, Three-dimensional calculation of bubble growth and drop ejection in a bubble jet printer, J. Fluids Eng. 114 (1992) 638–641.
[3] A. Asai, Bubble dynamics in boiling under high heat flux pulse heating, J. Heat Transfer 113 (1991) 973–978.
[4] P.H. Chen, W.C. Chen, S.H. Chang, Bubble growth and ink ejection process of a thermal ink jet printerhead, Int. J. Mech. Sci. 39 (1997) 683–695.
[5] L. Lin, A.P. Pisano, V.P. Carey, Thermal bubble formation on polysilicon micro resistors, ASME J. Heat Transfer 120 (1998) 735–742.
[6] Y. Iida, K. Okuyama, K. Sakurai, Boiling nucleation on a very small film heater subjected to extremely rapid heating, Int. J. Heat Mass Transfer 37 (1994) 2771–2780.
[7] L. Lin, Microscale thermal bubble formation: thermophysical phenomena and applications, Microscale Thermophys. Eng. 2 (1998) 71–85.
[8] W.J. Yang, K. Tsutsui, Overview of boiling on microstructures–macro bubbles from micro heater, Microscale Thermophys. Eng. 4 (2000) 7–24.
[9] J.H. Tsai, L. Lin, Transient thermal bubble formation on polysilicon microresistors, ASME J. Heat Transfer 124 (2002) 375–382.
[10] T. Okamoto, T. Suzuki, N. Yamamoto, Microarray fabrication with covalent attachment of DNA using bubble jet technology, Nature Biotechnol. Apr. 18 (4) (2000) 438–441.
[11] R.R. Darwin, I. Dimitri, A.A. Pierre, M. Andreas, Micro total analysis systems. 1. Introduction, theory, and technology, Anal. Chem. 74 (2002) 2623–2636.
[12] C.M. Ho, Fluidics the link between micro and nano sciences and technologies, Proc. 14 IEEE MEMS (2001) 375–384.
[13] A.A. Pierre, I. Dimitri, R.R. Darwin, M. Andreas, Micro total analysis systems. 2. Analytical standard operations and applications, Anal. Chem. 74 (2002) 2637–2652.
[14] D.R. Meldrum, M.R. Holl, Microscale bioanalytical systems, Science 297 (16) (2002) 1197–1198.
[15] V.P. Skripov, Metastable Liquids, John Wiley, New York, 1974, Chapters 4 and 6.
[16] J. Frenkel, Kinetic Theory of Liquids, Dover, New York, 1955.
[17] L. Rayleigh, Pressure due to collapse of bubbles, Philos. Mag. 94 (1917).
[18] M.S. Plesset, S.A. Zwick, The growth of vapor bubble in superheated liquids, J. Appl. Phys. 25 (1954) 493–500.
[19] A. Prosperetti, M.S. Plesset, Vapor bubble growth in a superheated liquid, J. Fluid Mech. 85 (1978) 349–368.